Three-Dimensional Quantitative Structure−Activity Relationship Study of the Inhibition of Na^+,K^+-ATPase by Cardiotonic Steroids Using Comparative Molecular Field Analysis†

Carol D. Farr,‡ Craig Burd,‡ Michael R. Tabet,‡ Xia Wang,§ William J. Welsh,§ and William J. Ball, Jr.*,‡

Department of Pharmacology and Cell Biophysics, University of Cincinnati College of Medicine, 231 Albert Sabin Way, Cincinnati, Ohio 45267-0575, and Department of Chemistry and Biochemistry, University of Missouri-St. Louis, St. Louis, Missouri 63121

Received July 19, 2001; Revised Manuscript Received October 22, 2001

ABSTRACT: Na^+,K^+-ATPase is a transmembrane protein that transports sodium and potassium ions across cell membranes during an activity cycle that uses the energy released by ATP hydrolysis. Cardiotonic steroids (digitalis) inhibit this activity and consequently produce a positive inotropic response in the heart. To identify the structural features of the steroids that are important for this inhibition, we have tested the inhibitory properties of 47 cardiotonic and hormonal steroids and developed a three-dimensional quantitative structure−activity relationship (3D-QSAR) model for the inhibition of Na^+,K^+-ATPase using comparative molecular field analysis (CoMFA). We also developed a 3D-QSAR model for the binding of digoxin to the murine anti-digoxin monoclonal antibody (mAb) 26-10 because we have previously shown that the environment of the binding sites of 26-10 and the enzyme are similar (Kasturi et al. (1998) *Biochemistry 37*, 6658−6666). These statistically predictive 3D-QSAR models indicate that both binding sites are about 20 Å long and have a close fit or complementarity about the β side of the lactone ring of digitalis. Furthermore, steric bulk about the lactone ring and the α sugar may be critical for drug binding. However, the binding site of Na^+,K^+-ATPase differs from that of mAb in that it has a greater number of electrostatic interactions along the α-sugar, steroid, and lactone moieties. In addition, the availability of the structure of the 26-10 Fab−digoxin complex (Jeffrey et al. (1993) *Proc. Natl. Acad. Sci. U.S.A. 90*, 10310−10314) enabled us to compare the CoMFA-derived contour maps with the known locations for amino acid residues comprising the mAb ligand binding site.

Na^+,K^+-ATPase[1] is a heterodimeric transmembrane protein that transports sodium and potassium ions across cell membranes using energy from the hydrolysis of ATP. During its ion pumping cycle, the protein alternates between an ATP-bound E_1 conformation, with a cytosolic high-affinity cation binding site for sodium ions, and a phosphorylated E_2 conformation, with an extracellular high-affinity site for potassium ions. Its regulation of Na^+ and K^+ levels contributes to many essential cellular processes, including maintenance of the membrane potential for muscle contraction and nerve propagation, regulation of cell volume, and transport of other ions, amino acids, neurotransmitters, and glucose (*1*−*4*).

Digoxin and digitoxin are well-known examples of cardiotonic steroids (digitalis) that bind to the extracellular surface of the α subunit of the enzyme and inhibit its ATPase activity. In myocardial cells, this inhibition results in the sequential increase of cytosolic sodium and calcium concentrations and thereby increases the force of contraction. For this reason, these two compounds (especially digoxin) are widely used as inotropic agents for the treatment of congestive heart failure (CHF) (*5*). Unfortunately, digoxin has a low therapeutic index and can cause toxic effects (*6*), such as arrhythmias and ventricular fibrillations. Therefore, antigen-binding fragments (Fabs) of sheep anti-digoxin antibodies (Abs) are used as antidotes for digoxin overdoses, and anti-digoxin Abs are used in clinical assays to monitor serum levels of digoxin (*7*, *8*).

Clearly, understanding the structural features of complex formation between digoxin and its receptor, Na^+,K^+-ATPase, or with anti-digoxin Abs could lead to the development of inotropic drugs with larger therapeutic indices or Abs with greater specificity that could be used as improved antidotes.

Digoxin is composed of a cardiotonic steroid moiety with the A−B and C−D rings joined in a cis nonhormonal

† Support for this work came from the American Heart Grant-in-Aid, Southern and Ohio Valley Affiliate (W.J.B.), NIH Grant RO1-06312 (W.J.W), and NIH Training Grant 5 T32 HL07382 (C.F.; P.I., A. Schwartz).

* To whom correspondence should be addressed. Phone: (513) 558-2388. Fax: (513) 558-6911. E-mail: William.Ball@uc.edu.

‡ University of Cincinnati.

§ University of Missouri-St. Louis.

[1] Abbreviations: 3D, three-dimensional; AO, anthroylouabain; CDR, complementarity determining region; CoMFA, comparative molecular field analysis; Fabs, antigen-binding fragments; H, heavy chain; IC_{50}, concentration required to reduce enzyme activity by 50%; L, light chain; mAb, monoclonal antibody; Na^+,K^+-ATPase, magnesium-dependent and sodium- and potassium-activated adenosine triphosphatase; PCs, principal components; PLS, partial least squares; QSAR, quantitative structure−activity relationship; rel inh, relative inhibition calculated as ratio of IC_{50} for inhibitor to IC_{50} for digoxin; SDS−PAGE, sodium dodecyl sulfate−polyacrylamide gel electrophoresis; SD × coeff, standard deviation of column values multiplied by the corresponding equation coefficient.

10.1021/bi011511g CCC: $22.00
Published on Web 12/29/2001

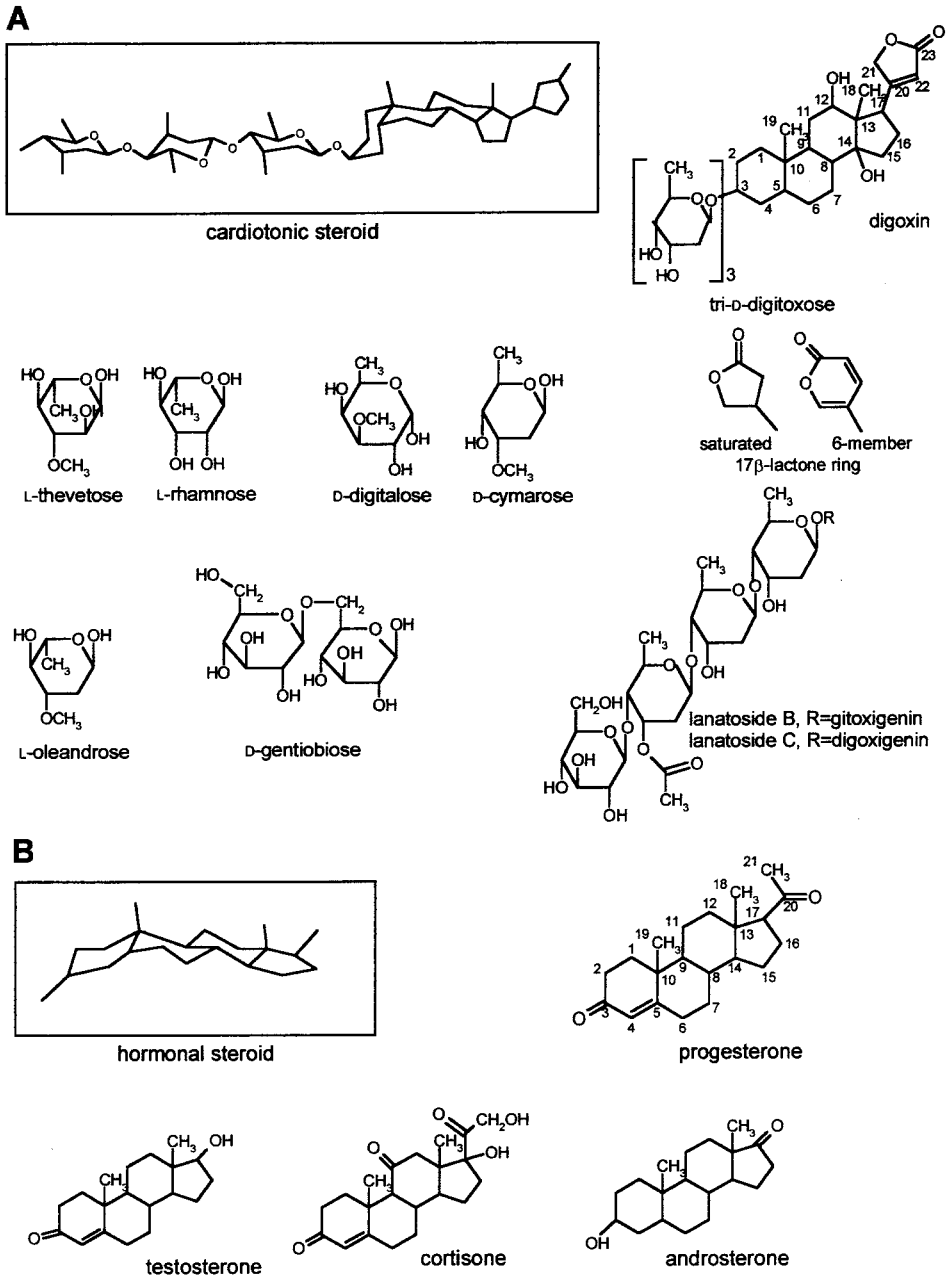

FIGURE 1: Structures of the cardiotonic steroids and hormonal steroids. (A) The structure of digoxin (boxed), illustrating the cis−trans−cis conformation and selected sugar and lactone ring substitutions from Table 2A. (B) The structure of progesterone (boxed), illustrating the all-trans conformation and representative hormonal steroids from Table 2B.

envelope configuration, while the B−C rings are joined in a flattened trans arrangement (*9*). Digoxin also has an α,*β*-unsaturated lactone ring attached at C-17 and three *β*(1,4)-D-glycoside-linked digitoxoses attached at C-3 (Figure 1A). There are many related compounds of plant and animal origin that have substitutions at various positions on the steroid rings, including different numbers and categories of carbohydrates at C-3 and variations in the saturation and size of the lactone ring. The importance of these various moieties in forming receptor−ligand complexes is not fully understood. Furthermore, little is known about the three-dimensional (3D) structure of Na^+,K^+-ATPase, the location of the cardiotonic steroid binding site, the causes of the toxic versus the therapeutic effects, or the molecular mechanism of enzyme inhibition.

Several approaches are used to characterize the binding site for the cardiotonic steroids and their mechanism of inhibition of Na^+,K^+-ATPase. Studies of photoaffinity labels, chemical modification, and α-subunit chimeras have all indicated that the binding site resides on the extracellular surface of the α subunit (*10*−*19*). Studies with site-directed and random mutagenesis of the sheep Na^+,K^+-ATPase α1 isoform have identified many amino acids that are involved with the binding of cardiotonic steroids and the inhibition of ATPase activity (*20*−*28*). Enzyme inhibition studies have identified a basic lead structure (5*β*,14*β*-androstane-3*β*,14-diol) as the minimum moiety required for cardiotonic steroid recognition by the enzyme (*29*).

The binding of cardiotonic steroids to spontaneous mutants of murine anti-digoxin monoclonal antibodies (mAbs) has also been studied (*30*). The structure of two Fabs bound with digoxin or ouabain has been determined with X-ray crystallography (*31*, *32*). Further, we have used anthroylouabain (AO) and spectroscopic techniques to show that the binding

site for digitalis on Na^+,K^+-ATPase has a structural environment similar to that on the murine anti-digoxin mAb 26-10 (*33*). Comparison of the information about receptor−ligand complex formation for the enzyme and mAbs may be useful because the ligand presents the same structural features in both cases (*34*).

Structure−activity studies of the inhibition of Na^+,K^+-ATPase by cardiotonic compounds have generated large databases of $-\Delta G°$ values (*35*−*37*). In this paper, we present a new approach to investigate the interaction of these compounds with their receptor. Recently, 3D quantitative structure−activity relationship (3D-QSAR) models have been produced with comparative molecular field analysis (CoMFA) and used to describe receptor−drug complexes at a molecular level by correlating the structures of related ligands with their biological activity (*38*). CoMFA has been used to examine receptor−ligand interactions for drug design and for other QSAR applications (*39*−*45*).

In this study, we examined the inhibition of Na^+,K^+-ATPase by 47 cardiotonic or hormonal steroids and produced a 3D-QSAR model that identifies the steric and electrostatic fields of the ligands that are most important to this inhibition. We also report that some of the fields that are important for enzyme inhibition are similar to those that are important for the binding of ligands to 26-10. In addition, by virtue of the excellent correlation between these fields and the position of specific residues in the complementarity determining regions (CDRs), as established by X-ray crystallography, we propose that the identification and visualization of these fields for Na^+,K^+-ATPase will contribute to the determination of the binding site for cardiotonic steroids and the mechanism of their inhibitory effects.

MATERIALS AND METHODS

Na^+,K^+-ATPase Isolation and Characterization. Na^+,K^+-ATPase was purified from the outer medulla of frozen lamb kidney using the method of Lane et al. (*46*) and had an initial ATPase activity of ∼1100 μmol mg^{-1} h^{-1}. The protein concentration was determined by the Lowry procedure (*48*) using BSA as the protein standard. A sample from the final preparation was subjected to SDS−PAGE (8% gel) and produced only two protein bands: one at 110 kDa and the other at 55 kDa when stained with Coomassie blue.

Inhibition of Na^+,K^+-ATPase Activity. The inhibition of Na^+,K^+-ATPase activity by cardiotonic and hormonal steroids was determined with modifications of a previously described assay (*48*) using a UVIKON 930 spectrophotometer. Initially, Na^+,K^+-ATPase preparation, without or with varying concentrations of inhibitor (prepared in ethanol, methanol, distilled water, or chloroform), was incubated for 30 min at 37 °C in the assay mixture (40 nM L-histidine, 10 mM $MgCl_2$, 100 mM NaCl, 10 mM KCl, 1 mM phosphoenol pyruvate (pH 7.3), ∼0.3 mM NADH, and pyruvate kinase-lactic dehydrogenase (pH 7.3)). After the background NADPH oxidation rate was determined for 10 min, the Na^+,K^+-dependent ATPase reaction was started with the addition of ATP to achieve a 5 mM concentration. All of the inhibitors decreased the activity of the enzyme to 90% or greater, and incubation times up to 60 min did not increase the potency of inhibition beyond that achieved with the 30 min preincubation.

The IC_{50} values were determined by plotting the percent activity as a function of the log [inhibitor]. The data points were fit with a four-parameter logistic equation, using Kaleidagraph (Synergy Software, Reading, PA) in order to monitor any variations in the slopes of the inhibition curves. The values for the Hill coefficients were randomly centered at about 1. The relative inhibition (rel inh) values were calculated as the ratio of the IC_{50} values of the inhibitors to those for digoxin.

Training Sets for 3D-QSAR Analysis. The training set (i.e., data set) used to construct the 3D-QSAR model for the inhibition of Na^+,K^+-ATPase by cardiotonic and hormonal steroids was based on our determinations of rel inh values. The training set for the binding of ligands to 26-10 is based on the ratio of inhibitory concentration values for 34 compounds, determined by a competition radioimmunoassay and reported previously by Schildbach et al. (*30*). To be consistent with other QSAR studies, the rel inh values were converted so that larger activity values represented more potent inhibitors relative to digoxin. The training set data point for each competitor was calculated as log [100 × (IC_{50} of digoxin/IC_{50} of inhibitor)]. For both training sets, the value for digoxin is 2 (log 100), and inhibitors with less inhibitory effect or lower affinity have lower values.

Two 3D-QSAR models were constructed for each receptor. For the first model in each case (Model I), the data set was divided into a training set, for model development, and a test set, for model validation. The second model (Model II) was constructed after the training and test sets were combined.

Molecular Modeling. The 3D structure of each compound was built using the molecular fragment library of Sybyl 6.6 (Tripos, Inc., St. Louis, MO) on a Silicon Graphics workstation. The structure of each cardiotonic steroid was based on the structure of digoxin, bound to murine Fab 26-10, as determined by X-ray crystallography (*31*), and available (identification number 1IGJ) from the Protein Data Bank (PDB). The structure of each hormonal steroid was based on the structure of progesterone, bound to Fab'DB3, determined by X-ray crystallography (*49*), and available (identification number 1DBB) in the PDB. Because Jeffrey et al. did not observe any electron density for the two terminal digitoxoses in the structure of digoxin (*31*), two digitoxose sugars were added to the PDB structure, using the molecular fragments library in Sybyl, and the global minimum-energy conformation was determined. The global minimum-energy conformation was identified using the following steps: (1) optimize the geometry of each molecule to the local minimum-energy conformation using an energy gradient of 0.001 kcal/(mol Å), (2) search all of the rotatable bonds in 10° increments to locate minimum-energy torsion angles, and (3) reoptimize the molecules to their lowest minimum-energy conformation using the bond angles established in step two. The energy-minimized digoxin structure was modified with the (Sybyl) molecular fragments library to build the remaining cardiotonic steroid structures. A global minimum-energy conformation was also determined for thevetin B because the 1−6 glycosidic bonds created a twisted carbohydrate chain. Similarly, the progesterone structure was modified to build the additional steroid structures. Finally, all of the structures were energy-minimized using the Tripos force field with a distance-

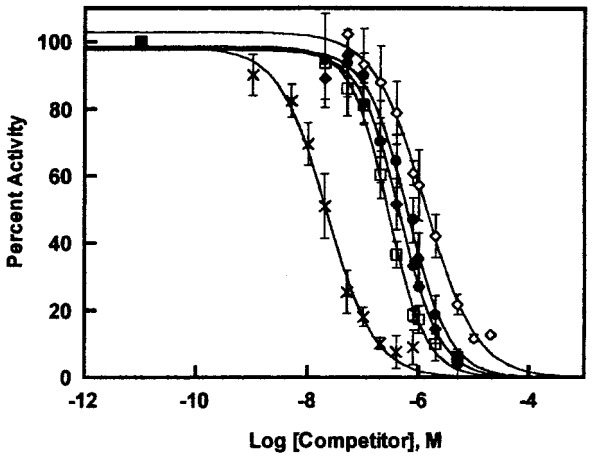

FIGURE 2: Inhibition of Na^+,K^+-ATPase by various cardiotonic steroids: bufalin (×), digoxigenin monodigitoxose (□), digoxigenin bisdigitoxose (◆), digoxin (●), and gitoxin (◇). Error bars represent the standard deviation of 3−5 data points.

dependent dielectric function ($\epsilon = \epsilon_0 r$, where $\epsilon_0 = 1$) and a convergence criterion of 0.001 kcal/mol energy difference between successive iterations. The Gasteiger−Marsili method was used to calculate the atomic partial charges (*50*). Although there can be rotation about the glycoside (C-3, O) and lactone-cardenolide (C-17 to C-20) bonds and some of the compounds may assume alternate steroid ring A conformations (*51*), we assumed the energy-minimized conformation for each compound with each receptor. We evaluated the contour maps, with the understanding that a C-3 or C-17 rotation may have occurred (*31*).

Comparative Molecular Field Analysis (CoMFA) Alignment. To align the compounds, we matched the B and C rings (C-5 to C-14) of each cardiotonic and hormonal steroid to the corresponding atoms in digoxin, using a least-squares fit. Therefore, the B and C rings, joined in trans, served as the scaffolding of the pharmacophoric elements. The aligned compounds used for the model of the inhibition of Na^+,K^+-ATPase are shown in Figure 3A, and those for the model of 26-10 ligand complex formation are shown in Figure 3B. Next, each compound was independently placed in a 3D grid with 2 Å spacing intervals. A carbon probe with an sp^3 configuration and a +1.0 charge was placed at each grid intersection, and the steric (van der Waals 6-12) and electrostatic (Coulombic) energies between the probe and compound were calculated for each intersection. The calculated energies greater than 30 kcal/mol were truncated to this value (*51*).

PLS-QSAR. Partial least-squares (PLS) regression was used to analyze the CoMFA results by correlating variations in the observed rel inh values with variations in the steric and electrostatic fields of the corresponding compound. The analysis generates a linear equation (*39*)

$$\text{Biological activity} = k + aS_1 + bS_2 + ... + mS_n + nE_1 + ... + zE_n \quad (1)$$

where k is a constant, $a-m$ are the coefficients for the steric (S) parameters, and $n-z$ are the coefficients for the electrostatic (E) parameters. A PLS cross-validation procedure ("leave-one-out"; LOO) combined and reduced the large number of steric and electrostatic field descriptors to a few

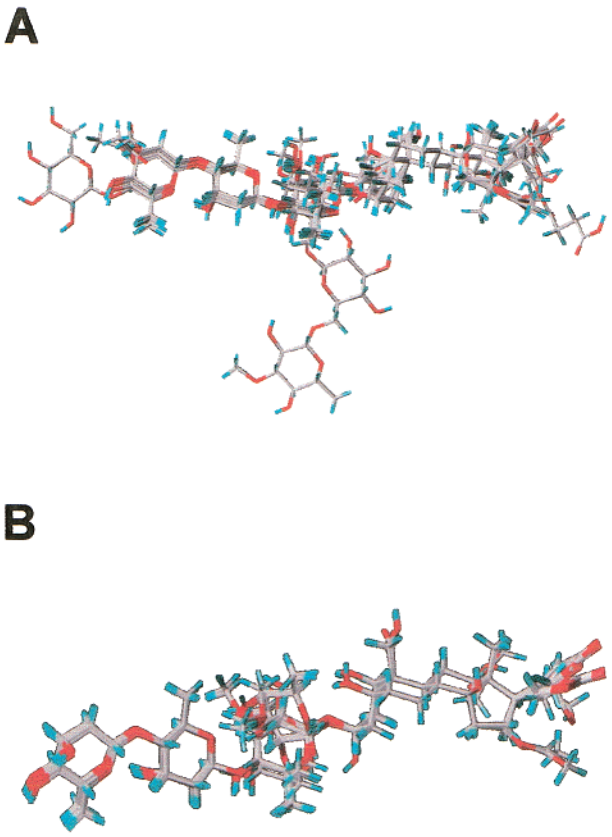

FIGURE 3: Ligand alignment used in 3D-QSAR studies for (A) Na^+,K^+-ATPase and (B) mAb 26−10.

principal components (PCs), which are linear combinations of the original descriptor variables. The cross-validated r^2 (termed q^2, hereafter; eq 2) shows how well the model-predicted values match the observed values,

$$q^2 = 1 - [\sum(y - y_{pred})^2 / \sum(y - y_{mean})^2] \quad (2)$$

where y, y_{pred}, and y_{mean} represent each observed value, each predicted value, and the mean descriptor value, respectively (*39*). An acceptable lower limit for the q^2 value for a model with the ability to predict the activity of untested compounds is 0.40 with values 0.4−0.5 being predictive and $q^2 > 0.5$ being strongly predictive (*41*). The final 3D-QSAR model was determined with the LOO-determined number of PCs and without cross-validation. The r^2 value (eq 3) shows the goodness of fit (i.e., the validity of the correlation between the calculated steric and electrostatic fields and the log value)

$$r^2 = 1 - [\sum(y - y_{cal})^2 / \sum(y - y_{mean})^2] \quad (3)$$

where y, y_{cal}, and y_{mean} represent each observed log value, each predicted log value based on the final 3D-QSAR equation, and the descriptor mean value, respectively. An $r^2 > 0.9$ is considered to be internally self-consistent (*41*).

The initial 3D-QSAR models developed for Na^+,K^+-ATPase inhibition included the entire 34 rel inh values, but this model did not meet an acceptable criteria ($q^2 > 0.4$; $r^2 > 0.9$). The removal of the two compounds (helveticoside and strophanthidin) with the largest residuals from the sets produced a q^2 value of 0.439, and the removal of a third

compound, acetylstrophanthidin, gave a value of 0.514. As a compromise between a smaller data set or higher q^2 value, we chose to delete just two compounds from Models I and II (see footnote e in Table 2A). Further testing indicated problems with our sample of helveticoside, and discussion of its results have been deleted. The initial 3D-QSAR model for digoxin binding to 26-10 used all the available data and did meet the q^2 and r^2 target values. Therefore, this model became the final Model II.

CoMFA Contour Maps. The steric and electrostatic CoMFA SD × coeff contour maps, generated with each 3D-QSAR model, identify the regions around the ligands where a change in the field parameters affects the ligand inhibition or binding activity. Specifically, at each lattice point, the SD of each field value at that point and the corresponding equation coefficient are multiplied together. If the product is higher than 80% or lower than 20% of all the calculated products, the point is color-coded and plotted. Green and yellow indicate regions where increased steric bulk corresponds to an increase or decrease in the activity, respectively. Red and blue indicate regions where an increase in the ligand's negative charge corresponds to an increase or decrease in the activity, respectively.

Reagents and Inhibitors. The inhibitors were obtained from the following companies: α-acetyldigoxin, 16-acetylgitoxin, dihydrodigitoxin, and evomonoside from Indofine (Somerville, NJ); cymarin, lanatoside B, and uzarigenin from Pfalz and Bauer (Waterbury, CT); digitoxigenin bisdigitoxose, digitoxigenin monodigitoxose, and digoxigenin bisdigitoxose from Roth Karlsruhe, Germany; digoxigenin monodigitoxose from Glaxo-Wellcome (Research Triangle Park, NC); acetyldigitoxin, 17α-hydroxyprogesterone-17-acetate 3-(*O*-carboxymethyl)oxime, acetylstrophanthidin, aldosterone, androsterone, bufalin, chlormadinone acetate, cholesterol, cinobufagin, corticosterone, cortisone, dehydrocortisone, dehydroisoandrosterone, digitoxigenin, digitoxin, digoxigenin, digoxigenin-3,12-diacetate, digoxin, dihydroouabain, β-estradiol, gitoxigenin, gitoxin, helveticoside, hydrocortisone, lanatoside C, neriifolin, oleandrin, ouabagenin, ouabain, prednisolone-21-acetate, prednisolone-21-hemisuccinate, progesterone, proscillaridin A, strophanthidin, testosterone, and thevetin B from Sigma-Aldrich Co. (St. Louis, MO). All other buffers and chemical reagents were purchased from Sigma Chemical Co.

RESULTS AND DISCUSSION

Characterization of Na^+,K^+-ATPase Inhibitors. We determined the ability of 47 cardiotonic and hormonal steroids to inhibit the Na^+- and K^+-dependent ATPase activity of Na^+,K^+-ATPase ($\alpha1\beta1$ isoform). The structures of some of the compounds are illustrated in Figure 1, and then all are fully described in parts A and B of Table 1. Representative activity inhibition curves are presented in Figure 2, and the IC_{50} values obtained under our ATPase assay conditions were 0.6 μM for digoxin and 0.14 μM for digitoxin. Because digoxin is the cardiotonic agent most widely used in the United States, it served as our reference compound, and the observed rel inh values (IC_{50} values relative to digoxin) for all the compounds are presented in Tables 2A and 2B. It should be noted that digoxin was not one of the better inhibitors. The most potent inhibitors were the bufadienolides (bufalin, cinobufagin, and proscillaridin A) with their six-membered rather than five-membered unsaturated lactone rings, linked at C-17β. Bufalin was 29-fold more potent than digoxin and was the most effective inhibitor.

The least potent inhibitors were two hormonal steroids: chlormadinone acetate and 17α-hydroxyprogesterone-17-acetate-3-(*O*-carboxymethyl)oxime (rel inh values of 8.4 and 320, respectively), and none of the other 12 hormonal steroids (as well as cholesterol) showed any activity with the enzyme (Table 2B). Therefore, we focused our attention on the cardiotonic compounds, while the two hormonal steroids that did inhibit the enzyme had the most complex chemical additions at the C-17 position and these modifications likely mimic some structural aspects of the lactone ring of the cardiotonic steroids. If the lactone double bond is saturated (dihydrodigitoxin), the inhibitory potency is reduced 5-fold. These results, together with the results of the bufadienolides, suggest that the lactone ring plays an important role in the inhibition of the enzyme.

Interestingly, and contrary to the broad range of affinities observed for the interactions of cardiotonic steroids with several murine anti-digoxin mAbs (*30*, *32*), the rel inh values for most of the cardiotonic steroids were within a single order of magnitude of each other. Therefore, the enzyme shows little fine-specificity of binding. Within this narrow range, some of the cardiotonic steroids can be grouped according to the specific modifications on their steroid moiety. Digitoxigenin (no sugars), which lacks the hydroxyl found at C-12 on digoxigenin, has the minimum number of substituents on the steroid moiety and is 4-fold more potent than digoxigenin. Digitoxin, neriifolin, and evomonoside, with different sugars at C-3, all have similar strong inhibitory effects (rel inh values of 0.1−0.2). Two additional digitoxigenin-related compounds have reduced inhibition values: thevetin B, with sugars joined 1−6 instead of 1−4, and uzarigenin, with a flattened A−B ring junction (rel inh values of 0.8). The fact that uzarigenin is only 4-fold less effective than digitoxigenin suggests that the presence of the lactone ring and cis conformation of the C−D rings, rather than the cis conformation of the A−B rings, is most important for its inhibitory effect.

Another group, the gitoxin-related compounds, have substitutions at C-16, and their inhibitory potencies depend on the modifications. Gitoxigenin is 6-fold less potent than digitoxigenin, while oleandrin, 16-acetylgitoxin, and gitoxin (one oleandrose or three digitoxoses at C-3) are 1-, 3-, and 9-fold less potent than digitoxin.

The final group of ouabagenin- and strophanthidin-related compounds is more soluble than either digoxin or digitoxin and used most frequently in research studies. The additional hydroxyls at C-1, C-5, C-11, and C-19 on ouabagenin reduce the potency 9-fold when compared to digitoxigenin, while the addition of an hydroxyl at C-5 and a keto group at C-19 on strophanthidin reduce the potency 2-fold.

The importance of the sugar moiety can be specifically evaluated by examining selected combinations of cardiotonic steroids. The most common sugar is digitoxose. If three digitoxoses are added to digitoxigenin, digoxigenin, and gitoxigenin, the inhibitory potency of each compound (digitoxin, digoxin, and gitoxin) actually decreases 1−2-fold. However, if rhamnose is added to digitoxigenin or ouabagenin, the inhibitory potencies increase 2-fold, while thevetose,

Table 1: Structural Characteristics of Cardiotonic and Hormonal Steroids

(A) Cardiotonic Steroids

	substitutions at steroid positions							
cardiotonic steroid	1β	3β	5β	11α	12β	16β	17β	19
Digoxigenin Base								
digoxin		tri-D-digitoxose			−OH			
α-acetyldigoxin		tri-D-digitoxose[a]			−OH			
lanatoside C		see Figure 1A			−OH			
12-acetyldigoxin[b]		tri-D-digitoxose			$-OCOCH_3$			
dihydrodigoxin[b]		tri-D-digitoxose			−OH		saturated	
digoxigenin bis-digitoxose		bis-D-digitoxose			−OH			
digoxigenin mono-digitoxose		D-digitoxose			−OH			
digoxigenin		−OH			−OH			
dihydrodigoxigenin[b]		−OH			−OH		saturated	
3-epidigoxigenin[b]		α-OH[c]			−OH			
digoxigenin-3,12-diacetate		$-OCOCH_3$			$-OCOCH_3$			
Digitoxigenin Base								
digitoxin		tri-D-digitoxose						
acetyldigitoxin (α:β, 2:1)		tri-D-digitoxose[a]						
dihydrodigitoxin		tri-D-digitoxose					saturated	
digitoxigenin bis-digitoxose		bis-D-digitoxose						
digitoxigenin mono-digitoxose		D-digitoxose						
evomonoside		L-rhamnose						
neriifolin		L-thevetose						
thevetin B		1 thevetose + 1(2 sugar) gentiobiose						
digitoxigenin		−OH						
acovenoside A[b]	−OH	6-deoxy-3-*O*-methyl-L-talose						
uzarigenin (trans A/B ring)		−OH	α-H					
Bufalin		−OH					six-membered	
cinobufagin		−OH	−OH			$-OCOCH_3$	six-membered	
cinobufagin								14−15 β-epoxide
proscillaridin A		L-rhamnose	4−5 double bond				six-membered	
Gitoxigenin Base								
gitoxin		tri-D-digitoxose				−OH		
diginatin[b]		tri-D-digitoxose			−OH	−OH		
gitaloxigenin[b]		−OH				-−OCHO		
gitaloxin[b]		tri-D-digitoxose				−OCHO		
16-acetylgitoxin		tri-D-digitoxose				$-OCOCH_3$		
gitoxigenin-3-acetate[b]		$-OCOCH_3$				−OH		
gitoxigenin-3,16-diacetate[b]		$-OCOCH_3$				$-OCOCH_3$		
gitoxigenin		−OH				−OH		
gitoxigenin mono-digitoxose[b]		D-digitoxose				−OH		
lanatoside B		see Figure 1A				−OH		
strospeside[b]		D-digitalose				−OH		
oleandrigenin mono-digitoxose[b]		D-digitoxose				$-OCOCH_3$		
oleandrin		oleandrose				$-OCOCH_3$		
oleandrigenin[b]		−OH				$-OCOCH_3$		
strophanthidol[b]		−OH	−OH					−OH
strophanthidin		−OH	−OH					=O
acetylstrophanthidin		$-OCOCH_3$	−OH					=O
cymarin		cymarose	−OH					=O
helveticoside		D-digitoxose	−OH					=O
ouabain	−OH	L-rhamnose	−OH	−OH				−OH
dihydroouabain	−OH	L-rhamnose	−OH	−OH			saturated	−OH
ouabagenin	−OH	−OH	−OH	−OH				−OH

(B) Hormonal Steroids

	substitutions at steroid positions					
hormonal steroid	3	4 to 5, 5 to 6, or 6 to 7 double bonds	6	11β	17	18
androsterone	α-OH	none			=O	
dehydroisoandrosterone[d]	β-OH	5−6			=O	
progesterone	=O	4−5			β-$COCH_3$	

Table 1 (Continued)

(B) Hormonal Steroids

hormonal steroid	substitutions at steroid positions: 3	4 to 5, 5 to 6, or 6 to 7 double bonds	6	11β	17	18
chlormadinone acetate	=O	4−5; 6−7	−Cl		α-$OCOCH_3$; β-$COCH_3$	
17α-hydroxyprogesterone-17-acetate 3-(*O*-carboxymethyl)oxime	$NOCH_2CO_2H$	4−5			α-$OCOCH_3$; β-$COCH_3$	
testosterone	=O	4−5			β-OH	
corticosterone	=O	4−5		−OH	β-$COCH_2OH$	
aldosterone[e]	=O	4−5		−OH	β-$COCH_2OH$	=O
dehydrocortisone[f]	=O	1−2; 4−5		=O	α-OH; β-$COCH_2OH$	
prednisolone-21-acetate	=O	1−2; 4−5		−OH	α-OH; β-$COCH_2OCOCH_3$	
prednisolone-21-hemisuccinate	=O	1−2; 4−5		−OH	α-OH; β-$COCH_2OCO(CH_2)_2COO^-$	
hydrocortisone	=O	4−5		−OH	α-OH; β-$COCH_2OH$	
cortisone	=O	4−5		=O	α-OH; β-$COCH_2OH$	
cholesterol	β-OH	5−6			β-$CH(CH_3)(CH_2)_3CH(CH_3)_2$	
β-estradiol[g]	−OH	aromatic A ring		β-OH		

[a] α or β $-OCOCH_3$ on terminal digitoxose C-3. [b] Analogues used only in Margolie's lab data set (*30*). [c] Note α orientation. [d] Prasterone. [e] In equilibrium with hemiacetal formed by C-11 hydroxyl and C-18 carboxyl. [f] Prednisone. [g] Note: no methyl on C-10.

when added to digitoxigenin, has no effect. We can also examine the effect of adding different sugars to the same aglycone. There is little effect in adding a single digitoxose, rhamnose, or thevetose to digitoxigenin (rel inh of 0.18); the rel inh values of the glycoside compounds are 0.22, 0.099, and 0.17, respectively. Also, the addition of a single cymarose sugar (forming cymarin) to strophanthidin has no effect.

Development of a 3D-QSAR Model for Inhibition of Na^+,K^+-ATPase by Digitalis. Next, we determined whether CoMFA could generate a 3D-QSAR model for the interaction of cardiotonic and hormonal steroids with Na^+,K^+-ATPase, despite the relatively narrow range of activities. For Model I, we used the rel inh values of 28 compounds and randomly excluded (16-acetylgitoxin, acetylstrophanthidin, lanatoside C, and thevetin B) so that they could serve as test compounds for the model. Model I ($q^2 = 0.500$; $r^2 = 0.967$ using five PCs) predicted the relative inhibitory values within 3−20% of their log(100/rel inh) values. These results demonstrated that a statistically predictive 3D-QSAR model could be generated.

The final 3D-QSAR Model II ($q^2 = 0.439$; $r^2 = 0.949$ using five PCs) utilized 32 compounds (Figure 4A). An illustration of the aligned structures of the inhibitors is shown in Figure 3A, and a plot of the correlation (r^2) between the calculated and the observed log(100/rel inh) values is presented in Figure 4A. The CoMFA generated contour maps for the steric and electrostatic fields are shown in Figure 5A, with digoxin inserted for reference. The steric field contribution to the model was 44%, while the electrostatic field contribution was 56%; thus, the electrostatic interactions make the larger contribution to the model.

The contour maps visualize the areas of the steric and electrostatic fields that are most important for explaining the variation in enzyme inhibition by this series of compounds. The addition of steric bulk to the region about the α sugar that is indicated by the green area in the upper contour map of Figure 5A improves the inhibitory ability of the ligand. The fact that the addition of digitoxose, in contrast to other sugars tested, decreased ligand potency probably accounts for the presence of the yellow contour region (decreasing potency) that is contained within the green area. There is also a green region near the lactone ring that is consistent with the result that bufalin-related compounds were the most potent inhibitors. The small yellow regions scattered about the steroid's C and D rings show regions where the fit between the inhibitor and the enzyme may already be optimal and any increase in bulk, especially about C-16 and the C-18 methyl group, decreases the ability of the ligand to inhibit the enzyme.

The red regions in the electrostatic (lower) contour map (Figure 5A) are located about the ligand from the α-sugar ring and its C-3 link, along the steroid and especially around the lactone ring. The red regions highlight areas where an increased electronegativity on the ligand should increase inhibition. There are three blue regions where a decrease in electronegativity of the ligand should increase inhibition; two are located near the α sugar, and one region is found above the hydroxyl at C-12.

Development of a 3D-QSAR Model and Contour Map for Digoxin Binding to mAb 26-10. Because we have previously used spectroscopic methods to show that there are similarities between the digitalis binding sites of the enzyme and mAb 26-10 (*33*), we also determined whether binding affinity data, already available from studies by Schildbach et al. (*30*), for 26-10 could be used to generate a 3D-QSAR model. Initially, we generated 3D-QSAR Model I ($q^2 = 0.595$; $r^2 = 0.951$ using five PCs) with CoMFA using the binding data for 31 inhibitors, while excluding three compounds (acovenoside A, gitoxigenin-monodigitoxose, and oleandrin) as test compounds. This initial model was able to predict the rel inh values of the test compounds within 12%, 4%, 43% of their observed log(100/ratio of inh conc.) values, respectively.

For the final model II ($q^2 = 0.629$; $r^2 = 0.948$ using five PCs), we used all 34 compounds and obtained an excellent predictive model. The contributions from the steric and electrostatic fields were 58% and 42%, respectively. These results indicate that steric interactions contribute the most to the variation in ligand binding affinities and are essentially the reverse of those in the Na^+,K^+-ATPase model, where the steric components were only 44%. The reduced role for electrostatic interactions between digoxin and 26-10 is

Table 2: Relative Inhibition Values of Cardiotonic and Hormonal Steroids

(A) Relative Inhibition Values of Cardiotonic Steroids for Sheep Kidney Na^+,K^+-ATPase and Ratio of Inhibitory Concentrations of Cardiotonic Steroids for Cardiotonic Steroids for Binding to Murine mAb 26-10

cardiotonic steriods	sheep kidney Na^+,K^+-ATPase rel inh[a]	murine mAb 26-10 ratio of inhibitory concentrations[b]
12-acetyldigoxin	nd[c]	160
α-acetyldigoxin	1.4 ± 0.005	nd
acetyldigitoxin	0.41 ± 0.04	nd
16-acetylgitoxin	0.65 ± 0.08	150
3-epidigoxigenin	nd	4
acetylstrophanthidin	0.29 ± 0.01	2
acovenoside A	nd	2
bufalin	0.034 ± 0.004	nd
cinobufagin	0.14 ± 0.004	nd
cymarin	0.39 ± 0.03	1
diginatin	nd	2
digitoxigenin	0.18 ± 0.02	2
digitoxigenin bisdigitoxose	0.15 ± 0.01	nd
digitoxigenin monodigitoxose	0.22 ± 0.02	nd
digitoxin	0.24 ± 0.04	1
digoxigenin	0.78 ± 0.13	2
digoxigenin-3,12-diacetate	120 ± 10	750
digoxigenin bisdigitoxose	0.63 ± 0.06	1
digoxigenin monodigitoxose	0.44 ± 0.02	1
digoxin	1.0 ± 0.1	1
dihydrodigitoxin	1.1 ± 0.1	nd
dihydrodigoxigenin	nd	1700
dihydrodigoxin[d]	nd	1300
dihydroouabain	1.7 ± 0.1	nd
evomonoside	0.099 ± 0.005	3
gitaloxigenin	nd	150
gitaloxin	nd	30
gitoxigenin	1.0 ± 0.004	13
gitoxigenin-3,16-diacetate	nd	36000
gitoxigenin-3-acetate	nd	12
gitoxigenin monodigitoxose	nd	4
gitoxin	2.2 ± 0.2	5
helveticoside	19 ± 1[e]	1
lanatoside B	0.80 ± 0.04	nd
lanatoside C	1.3 ± 0.2	nd
neriifolin	0.17 ± 0.005	2
oleandrigenin	nd	17000
oleandrigenin monodigitoxose	nd	770
oleandrin	0.35 ± 0.01	740
ouabagenin	1.6 ± 0.07	50
ouabain	1.0 ± 0.1	35
proscillaridin A	0.13 ± 0.002	nd
strophanthidin	0.37 ± 0.07[e]	2
strophanthidol	nd	2
strospeside	nd	5
thevetin B	0.81 ± 0.05	nd
uzarigenin	0.76 ± 0.05	nd

(B) Relative Inhibition Values of Hormonal Steroids for Sheep Kidney Na^+,K^+-ATPase

hormonal steroids	sheep kidney Na^+,K^+-ATPase rel inh[f]
aldosterone	ni[g]
androsterone	ni
chlormadinone acetate	8.4 ± 0.1
cholesterol	ni
corticosterone	ni
cortisone	ni
dehydrocortisone	ni
dehydroisoandrosterone	ni
β-estradiol	ni
hydrocortisone	ni
prednisolone-21-hemisuccinate	ni
prednisolone-21-acetate	ni
progesterone	ni
17-α-hydroxyprogesterone-17-acetate-3-(*O*-carboxymethyl)oxime	320 ± 160
testosterone	ni

[a] Values are the average values from 2 to 9 independent experiments, and the error is the average deviation. [b] Reference *30*. [c] nd, not determined. [d] Reference *58*. [e] These compounds were left out of the final model (see text). [f] Values are the average values from 2 to 9 (average 2.5) independent experiments, and the error is the average deviation of those values. [g] ni, no inhibition at concentrations <1 μM.

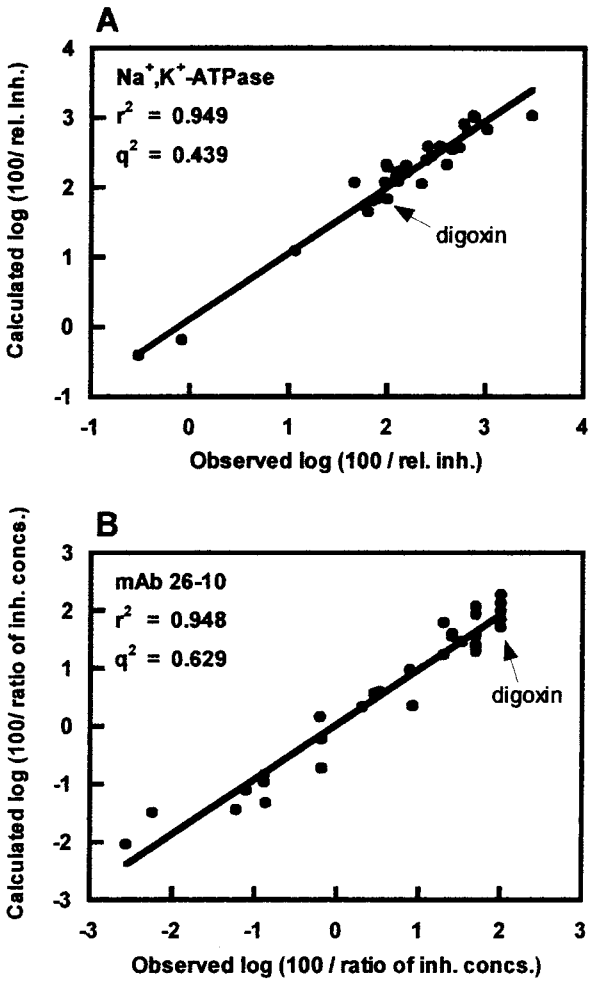

FIGURE 4: Comparison of the observed and calculated values for the (A) rel inh of Na^+,K^+-ATPase and (B) ratio of inhibitory concentrations (inh concn) for 26-10.

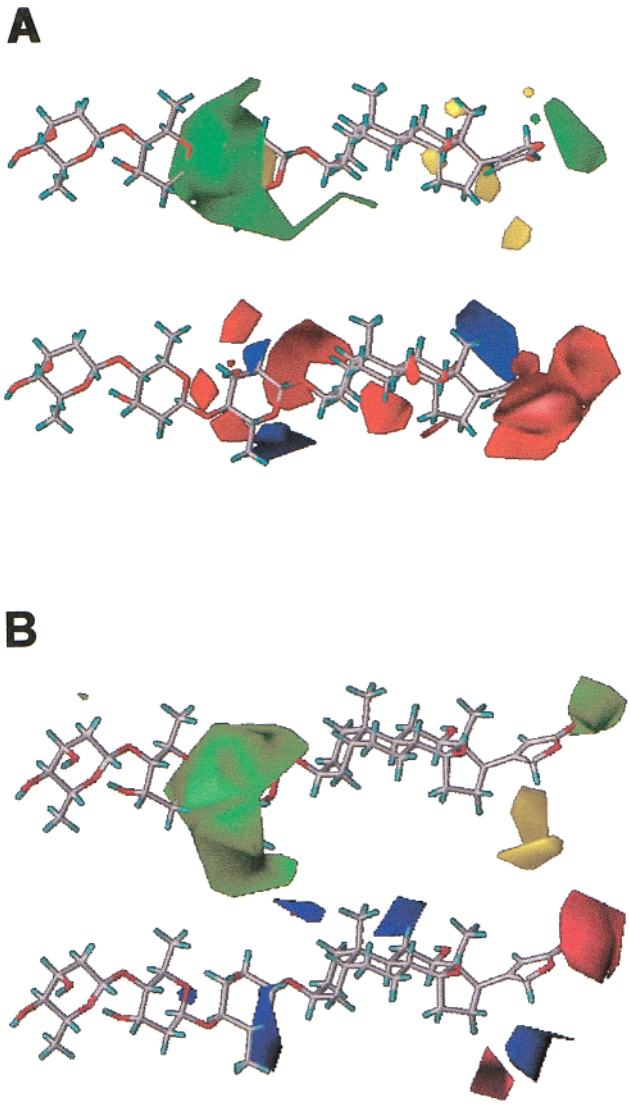

FIGURE 5: 3D-QSAR maps for (A) Na^+,K^+-ATPase and (B) mAb 26-10. The colored areas are the regions where the addition of steric bulk increases (green) or decreases (yellow) the activity. Also shown are regions where increase in electronegativity increases (red) or decreases (blue) the activity.

consistent with the conclusion of Jeffrey et al. (*31*) that shape complementarity is largely responsible for the high affinity of 26-10 for digoxin. They found no hydrogen bonds or salt links that contribute to complex formation.

The steric (upper) contour map (Figure 5B) for 26-10 shows a large green region that sweeps around the α and middle (β) sugar. This reflects the fact that the addition of tridigitoxose (or monodigitoxose or monorhamnose) to digitoxigenin, digoxigenin, gitoxigenin (or strophanthidin or ouabagenin) improves the affinity of the ligand 2−3-fold. The addition of tridigitoxose to gitaloxigenin improves the affinity 5-fold, and impressively, the addition of monodigitoxose or mono-oleandrose to oleandrigenin improves the affinity 22- to 23-fold, respectively. There is also a green region near the lactone. The yellow region beneath the lactone ring shows an area where there is a close fit between the ligand and mAb, and the addition of bulk in this region decreases the affinity. These results reflect the dramatic 1300- and 1700-fold reduction in binding affinity of dihydrodigoxin and dihydrodigoxigenin that is probably due to the reorientation of the lactone ring upon saturation. In addition, there is a 3000-fold reduction in binding affinity when an acetate group is added at C-16 (gitoxigenin-3,16-diacetate).

Encouragingly, despite the more than 1000-fold difference between the IC_{50} value (0.6 μM) for inhibition of enzyme activity by digoxin (low-affinity conditions) and high affinity of digoxin (<1 nM) for 26-10 (*30*) and despite the overlapping but nonidentical test sets, the steric (upper) contour maps for Na^+,K^+-ATPase (Figure 5A) and 26-10 (Figure 5B) appear similar. Both contour maps have large green regions about the α sugar and the lactone ring and a yellow region on the β side of the lactone and steroid D ring. In our previous studies, results for both the enzyme−AO and 26-10−AO complexes showed that the anthroyl moiety, possibly substituting for the β sugar is not exposed to solvent. Rather, it binds in a hydrophobic environment and has close interactions with tryptophan residue(s). In addition, AO has an improved binding affinity with 26-10 over that of ouabain.

However, the electrostatic (lower) contour maps of 26-10 (Figure 5B) and Na^+,K^+-ATPase are different. For 26-10, there are a few scattered regions about digoxin where increased electronegativity decreases its binding. For the enzyme, there are several sites about the α sugar, steroid, and lactone where an increased electronegativity enhances binding. Both maps do, though, show that the addition of electronegativity near the lactone ring improves both ligand binding to 26-10 and its inhibition of the enzyme.

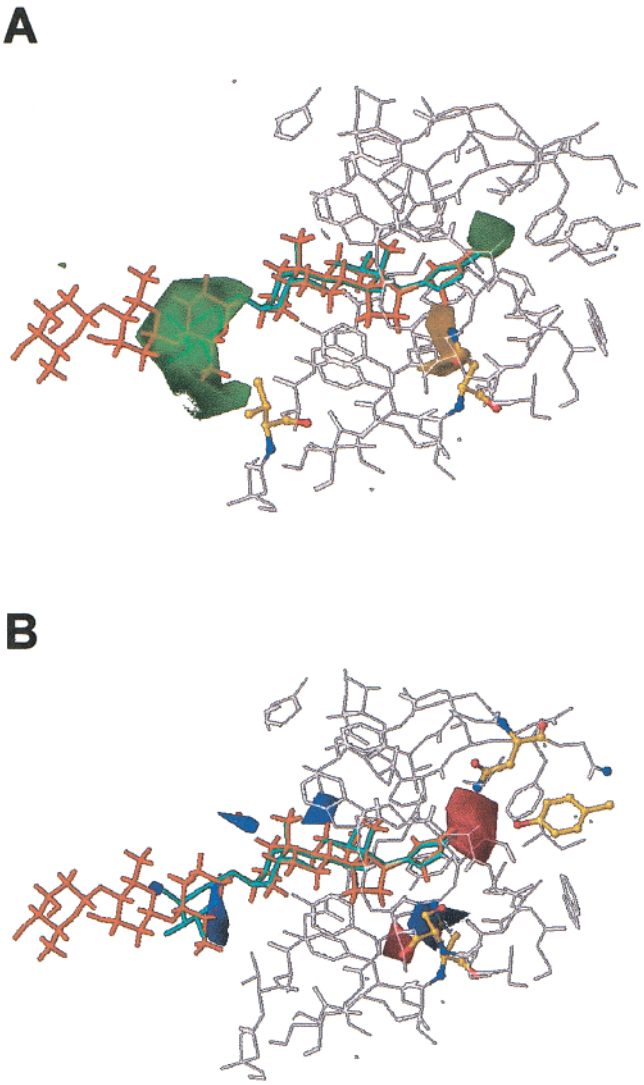

FIGURE 6: Comparison of the 3D-QSAR contour maps with the corresponding regions of the Fab 26-10−digoxin complex: (A) steric contour plot and (B) electrostatic contour plot.

We have been able to further investigate the mAb−ligand interactions by aligning the digoxin molecule in our CoMFA contour maps with digoxin in the crystal structure of Fab 26-10−digoxin complex (*31*). This superimposes the contour maps on the residues in the complementarity determining regions (CDRs) of Fab 26-10 (parts A and B of Figure 6) and allows us to compare the location of the contour fields with the known locations of residues comprising the binding site. Interestingly, the steric contour map indicates that increased bulk in a region about the α sugar that appears to lie outside the binding pocket contributes to the binding interactions. This likely results because the sugars can rotate around the glycosidic bonds and generate several secondary sites of interaction, such as with Val-H56, but not necessarily establish any single position that is detected in the X-ray crystallographic imaging. This interaction is absent for aglycone binding to the mAb. The yellow region near C-16 predicts the observed decrease in the affinity of mAb for oleandrin (acetate at C-16) and for dihydrodigoxin and dihydrodigitoxin, which have saturated and reorientated lactone rings. The model shows an Asn-H35 near this region, which would restrict an increase in steric bulk and provide partial charges for interaction with the ligand (indicated by the red and blue areas on the electrostatic map). For digoxin (digitoxin and gitoxin), there is only a 2−3-fold decrease in affinity if the three digitoxoses are removed. However, for oleandrin, there is a ~20-fold decrease. If the inclusion of an acetate group at C-16 changes the orientation of the ligand in the binding site, then an increased interaction (although weak) with the α sugar may occur.

While no residues of the crystallized Fab were found to form hydrogen bonds with digoxin, the distances in the crystal structure may not be the precise distances for the fully solvated complex. There are several residues (e.g., Tyr-L36 and Asn-L34) that are close to O-21 and O-23 that have the potential to account for the electrostatic interactions indicated by the red region near the lactone if there is a slight change in its orientation. The blue regions near the steroid's A ring and C-12 could reflect the decreased affinity for ouabain and 12-acetyldigoxin. In the future, as we obtain additional information, this type of modeling should be able to lead to the prediction of the amino acids of Na^+,K^+-ATPase that are likely to interact with digitalis.

In this work, we have used CoMFA to generate, for the first time, a 3D-QSAR model and contour maps for the inhibition of Na^+,K^+-ATPase by cardiotonic and hormonal steroids. Although a number of investigations of digitalis structure−activity relationships for the inhibition of ATPase activity (*26*, *36*, *52*−*54*) have been performed, none of these studies employed a method of data analysis that was capable of correlating the results to specific chemical properties of the ligands or visualizing the structural features that are important for the receptor−ligand interactions. In addition, we generated a 3D-QSAR model and contour maps for the binding of ligands to 26-10. This model has enabled us to visualize the structural features of the ligands that are important for binding to mAb and to predict the activities of untested compounds.

The 3D-QSAR contour maps for digoxin inhibition of Na^+,K^+-ATPase do allow us to make some preliminary predictions of the enzyme's digitalis binding site. Currently, there are two prominent models for the cardiotonic steroid binding site on Na^+,K^+-ATPase: the Repke model (*2*) that places the bound ligand within the membrane at the interface of two α subunits formed by adjacent H1 and H2 transmembrane (TM) segments and the Lingrel model (*3*) that places bound digoxin across the extracellular exposed portions of the α subunit.

The full length of the digoxin molecule is approximately 30 Å (*2*), but our contour plots show that the steric and electrostatic fields surrounding the ligands that are important to enzyme inhibition cover approximately 20 Å (from the lactone ring to the α sugar). This is the same distance that Repke et al. suggest is the depth (19 Å) of the digitalis binding cleft (*2*). Although the crystal structure of Na^+,K^+-ATPase is not known, the structure of the closely related calcium pump of the sarcoplasmic reticulum has been determined by Toyoshima et al. (*55*). The calcium pump has 10 TM α-helical segments, and the grouping of these segments in the TM domain has a diameter of approximately 40 Å. This size could easily include a cardiotonic binding site with a diameter of 20 Å on the extracellular surface. Thus, on this issue our contour plots for Na^+,K^+-ATPase are compatible with either model.

In the crystal structure of the 26-10−digoxin complex (*31*), the lactone of digoxin fits deeply into a binding pocket with the α sugar residing at the edge of the entrance and the β and terminal (γ) sugars extending out into the solvent. This orientation gives the two terminal sugars considerable flexibility. We predict a similar orientation for the binding site of digoxin on Na^+,K^+-ATPase. However, this model does not rule out the possibility of some protein interactions with the β and γ sugars.

Overall, though, our results appear more consistent with the Lingrel model. Repke proposes that a series of five hydrophobic residues along the surface of a side of each of the H1 and H2 TM segments interact with the lactone and steroid rings forming the binding site. This should generate steric interactions along the length of the aglycone on both its α and β sides. Instead, we observe the steric interactions to be restricted to the α sugar and lactone and the electrostatic interactions to occur along the length of the entire ligand molecule. Also, random mutagenesis has thus far not indicated that any of the hydrophobic H1 and H2 TM residues are involved. Furthermore, there is only one Trp in the α-subunit H1 segment (W99), and it seems more likely that one or more of the Trps (W308, W883, W887, and W899) of the H3−H4 and H7−H8 extracellular loops would account for our observed interactions of Trps of the enzyme with the anthroyl group of AO than would W99.

Finally, it will be informative to develop an analogous 3D-QSAR model for digoxin binding to Na^+,K^+-ATPase under high-affinity binding conditions of $Mg^{2+}P_i$ or Na^+-Mg^{2+}ATP in the absence of any cycling of the enzyme through its well-known different conformations and the absence of K^+ which decreases the enzyme's affinity for digoxin and sodium. Under these binding conditions, the α sugar of the cardiotonic steroids causes a significant decrease in the ligand's (aglycone) dissociation rate and increases the affinity of digitalis about 20-fold, for both digitalis-sensitive and digitalis-insensitive (rodent enzyme) forms of the enzyme (*56*, *57*). For digitalis-sensitive forms of the enzyme, digoxin binding essentially becomes irreversible under high-affinity conditions. These studies, plus the completion of our ongoing efforts to generate 3D-QSAR models for digoxin binding to several of our human sequence mAbs that can be aligned with their determined amino acid sequences, should give us considerably more insight into the structural requirements for "receptor" binding of digitalis. The 3D-QSAR results should correlate with, but in their methodological approach be independent of, the structure−activity relationship information derived from site-directed mutagenesis studies of Na^+,K^+-ATPase.

ACKNOWLEDGMENT

We thank Elizabeth Collantes and Purabi Dey for their technical assistance and Dr. Michael Margolies for permission to use his data for mAb 26-10.

REFERENCES

1. Thomas, R., Gray, P., and Andrews, J. (1990) *Adv. Drug Res. 19*, 311−562.
2. Repke, K. R. H., Sweadner, K. J., Weiland, J., Megges, R., and Schön, R. (1996) *Prog. Drug Res. 47*, 9−52.
3. Lingrel, J. B., Argüello, J. M., van Huysse, J., and Kuntzweiler, T. A. (1997) *Ann. N.Y. Acad. Sci. 834*, 194−206.
4. Blanco, G., and Mercer, R. W. (1998) *Am. J. Physiol. 275*, F633−F650.
5. The Digitalis Investigation Group (1997) *N. Engl. J. Med. 336*, 525−533.
6. Repke, K. R. H. (1997) *Drug Discovery Today 2*, 110−116.
7. Antman, E. M., Wenger, T. L., Butler, V. P., Haber, E., and Smith, T. W. (1990) *Circulation 81*, 1744−1752.
8. Butler, V. P., and Chen, J. P. (1967) *Proc. Natl. Acad. Sci. U.S.A. 57*, 71−78.
9. Go, K., Kartha, G., and Chen, J. P. (1980) *Acta Crystallogr. B36*, 1811−1819.
10. Forbush, B., III, Kaplan, J. H., and Hoffman, J. F. (1978) *Biochemistry 17*, 3667−3676.
11. Rossi, B., Vuilleumier, P., Gache, C., Balerna, M., and Lazdunski, M. (1980) *J. Biol. Chem. 255*, 9936−9941.
12. Jørgensen, P. L., Karlish, S. J. D., and Gitler, C. (1982) *J. Biol. Chem. 257*, 7435−7442.
13. Forbush, B., III. (1983) *Curr. Top. Membr. Transp. 19*, 167−201.
14. Hall, C. C., and Ruoho, A. E. (1983) *Curr. Top. Membr. Transp. 19*, 265−270.
15. Goeldner, M. P., Hirth, C. G., Rossi, B., Ponzio, G., and Lazdunski, M. (1983) *Biochemistry 22*, 4685−4690.
16. Ishii, T., and Takeyasu, K. (1993) *Proc. Natl. Acad. Sci. U.S.A. 90*, 8881−8885.
17. Blostein, R., Zhang, R., Gottardi, C. J., and Caplan, M. J. (1993) *J. Biol. Chem. 268*, 10654−10658.
18. Antolovic, R., Linder, D., Hahnen, J., and Schoner, W. (1995) *Eur. J. Biochem. 227*, 61−67.
19. Antolovic, R., Schoner, W., Geering, K., Canessa, C., Rossier, B. C., and Horisberger, J.-D. (1995) *FEBS Lett. 368*, 169−172.
20. Price, E. M., and Lingrel, J. B. (1988) *Biochemistry 27*, 8400−8408.
21. Price, E. M., Rice, D. A., and Lingrel, J. B. (1989) *J. Biol. Chem. 264*, 21902−21906.
22. Price, E. M., Rice, D. A., and Lingrel, J. B. (1990) *J. Biol. Chem. 265*, 6638−6641.
23. Canessa, C. M., Horisberger, J.-D., Louvard, D., and Rossier, B. C. (1992) *EMBO J. 11*, 1681−1687.
24. Schultheis, P. J., and Lingrel, J. B. (1993) *Biochemistry 32*, 544−550.
25. Askew, G. R., and Lingrel, J. B. (1994) *J. Biol. Chem. 269*, 24120−24126.
26. Palasis, M., Kuntzweiler, T. A., Argüello, J. M., and Lingrel, J. B. (1996) *J. Biol. Chem. 271*, 14176−14182.
27. Croyle, M. L., Woo, A. L., and Lingrel, J. B. (1997) *Eur. J. Biochem. 248*, 488−495.
28. Shi, H. G., Mikhaylova, L., Zichittella, A. E., and Argüello, J. M. (2000) *Biochim. Biophys. Acta 1464*, 177−187.
29. Schönfeld, W., Weiland, J., Lindig, C., Masnyk, M., Kabat, M. M., Kurek, A., Wicha, J., and Repke, K. R. H. (1985) *Arch. Pharm. 329*, 414−426.
30. Schildbach, J. F., Panka, D. J., Parks, D. R., Jager, G. C., Novotny, J., Herzenberg, L. A., Mudgett-Hunter, M., Bruccoleri, R. E., Haber, E., and Margolies, M. N. (1991) *J. Biol. Chem. 266*, 4640−4647.
31. Jeffrey, P. D., Strong, R. K., Sieker, L. C., Chang, C. Y. Y., Campbell, R. L., Petsko, G. A., Haber, E., Margolies, M. N., and Sheriff, S. (1993) *Proc. Natl. Acad. Sci. U.S.A. 90*, 10310−10314.
32. Jeffrey, P. D., Schildbach, J. F., Chang, C. Y. Y., Kussie, P. H., Margolies, M. N., and Sheriff, S. (1995) *J. Mol. Biol. 248*, 344−360.
33. Kasturi, R., Yuan, J., McLean, L. R., Margolies, M. N., and Ball, W. J., Jr. (1998) *Biochemistry 37*, 6658−6666.
34. Jerne, N. K. (1974) *Ann. Immunol. 125C*, 373−389.
35. Schönfeld, W., Schönfeld, R., Menke, K.-H., Weiland, J., and Repke, K. R. H. (1986) *Biochem. Pharmacol. 35*, 3221−3231.
36. Beer, J., Kunze, R., Herrmann, I., Portius, H. J., Mirsalichova, N. M., Abubakirov, N. K., and Repke, K. R. H. (1988) *Biochim. Biophys. Acta 937*, 335−346.
37. Repke, K. R. H., Weiland, J., Megges, R., and Schön, R. (1993) *Prog. Med. Chem. 30*, 135−202.

38. Cramer, R. D., III, Patterson, D. E., and Bunce, J. D. (1988) *J. Am. Chem. Soc. 110*, 5959−5967.
39. Green, S. M., and Marshall, G. R. (1995) *TIPS 16*, 285−291.
40. Tong, W., Lowis, D. R., Perkins, R., Chen, Y., Welsh, W. J., Goddette, D. W., Heritage, T. W., and Sheehan, D. M. (1998) *J. Chem. Inf. Comput. Sci. 38*, 669−677.
41. Collantes, E. R., Xing, L., Miller, P. C., Welsh, and Profeta, S. (1999) *J. Agric. Food Chem. 47*, 5245−5251.
42. Tong, W., Perkins, R., Xing, L., Welsh, W. J., and Sheehan, D. M. (1997) *Endocrinology 138*, 4022−4025.
43. Gamper, A. M., Winger, R. H., Liedl, K. R., Sotriffer, C. A., Varga, J. M., Kroemer, R. T., and Rode, B. M. (1996) *J. Med. Chem. 39*, 3882−3888.
44. Imberty, A., Mollicone, R., Mikros, E., Carrupt, P.-A., Pérez, S., and Oriol, R. (1996) *Bioorg. Med. Chem. 4*, 1979−1988.
45. Shim, J.-Y., Collantes, E. R., Welsh, W. J., Subramaniam, B., Howlett, A. C., Eissenstat, M. A., and Ward, S. J. (1998) *J. Med. Chem. 41*, 4521−4532.
46. Lane, L. K., Potter, J. D., and Collins, J. H. (1979) *Prepr. Biochem. 9*, 157−190.
47. Lowry, O. H., Rosebrough, N. J., Farr, A. L., and Randall, R. J. (1951) *J. Biol. Chem. 193*, 265−275.
48. Schwartz, A., Allen, J. C., and Harigaya, S. (1969) *J. Pharmacol. Exp. Ther. 168*, 31−41.
49. Arevalo, J. H., Stura, E. A., Taussig, M. J., and Wilson, I. A. (1993) *J. Mol. Biol. 231*, 103−118.
50. Gasteiger, J., and Marsili, M. (1980) *Tetrahedron 36*, 3219−3228.
51. Kawamura, A., Abrell, L. M., Maggiali, F., Berova, N., Nakanishi, K., Labutt, J., Magil, S., Haupert, G. T., and Hamyln, J. M. (2001) *Biochemistry 40*, 5835−5844.
52. Ahmed, K., Rohrer, D. C., Fullerton, D. S., Deffo, T., Kitatsuji, E., and From, A. H. L. (1983) *J. Biol. Chem. 258*, 8092−8097.
53. Yoda, A. (1973) *Mol. Pharmacol. 9*, 51−60.
54. From, A. H. L., Fullerton, D. S., and Ahmed, K. (1990) *Mol. Cell. Biochem. 94*, 157−165.
55. Toyoshima, C., Nakasako, M., Nomura, H., and Ogawa, H. (2000) *Nature 405*, 647−655.
56. Wallick, E. T., Pitts, B. J. R., Lane, L. K., and Schwartz, A. (1980) *Arch. Biochem. Biophys. 202*, 442−449.
57. O'Brien, W. J., Wallick, E. T., and Lingrel, J. B. (1993) *J. Biol. Chem. 268*, 7707−7712.
58. Schildbach, J. F., Near, R. I., Bruccoleri, R. E., Haber, E., Jeffrey, P. D., Ng, S.-C., Novotny, J., Sheriff, S., and Margolies, M. N. (1993) *J. Biol. Chem. 268*, 21739−21747.

BI011511G